BNL-203379-2018-JAAM

Synchrotron-based ambient pressure X-ray photoelectron spectroscopy of hydrogen and helium

J. Zhong, J. A. Boscoboinik

To be published in "Applied Physics Letters"

March 2018

Center for Functional Nanomaterials

Brookhaven National Laboratory

U.S. Department of Energy

USDOE Office of Science (SC), Basic Energy Sciences (BES) (SC-22)

DISCLAIMER

Synchrotron-Based Ambient Pressure X-ray Photoelectron Spectroscopy of Hydrogen and Helium

Jian-Qiang Zhong[1], Mengen Wang[1,2], William H. Hoffmann[3], Matthijs A. van Spronsen[4*], Deyu Lu[1], J. Anibal Boscoboinik[1*]

[1] Center for Functional Nanomaterials, Brookhaven National Laboratory, Upton, NY 11973, USA.

[2] Department of Materials Science and Chemical Engineering, Stony Book University, Stony Brook, New York 11790, USA.

[3] Department of Chemical and Biomolecular Engineering, NC State University, Raleigh, NC 27695-7905, USA.

[4] Department of Chemistry and Chemical Biology, Harvard University, Cambridge, MA 02138, USA.

Abstract

Contrary to popular belief, it is possible to obtain X-ray photoelectron spectra for elements lighter than lithium, namely hydrogen and helium. The literature is plagued with claims of this impossibility, which holds true for lab-based X-ray sources. However, this limitation is merely technical and relates mostly to the low X-ray photoionization cross sections of the 1s orbitals of hydrogen and helium. In this letter we show that, using ambient pressure X-ray photoelectron spectroscopy (XPS), a bright-enough X-ray source allows the study of these elusive elements. This has important implications in the understanding of the limitations of one of the most useful techniques in materials science and moreover, it potentially opens the possibility of using XPS to directly study the most abundant element in the universe.

Introduction

From all the elements in the periodic table, hydrogen is arguably among the most important one. It is a prime candidate to fuel a sustainable society; it is key in organic chemistry and essential in biology.[1, 2] The importance of hydrogen makes it imperative to have analytical tools to detect and quantify it. Due to its single electron, hydrogen diffraction intensities for X-rays and electrons are weak. Furthermore, hydrogen does not have an Auger transition and, hence, is invisible in Auger electron spectroscopy. Finally, it is widely claimed to be undetectable with X-ray photoelectron spectroscopy (XPS), one of the most frequently used techniques in surface science, materials science, and catalytic research. For example, an excellent systematic review on the effect of the presence of hydrogen in the XPS shifts of a variety of compounds states "While XPS is recognized as a preeminent tool for surface chemical analysis, a major shortcoming is that it cannot see hydrogen directly."[3] Another excellent article by Stojilovic entitled "Why Can't We See Hydrogen in X-ray Photoelectron Spectroscopy?" nicely explains why most students misunderstand the reason for the apparent impossibility of doing XPS on elements lighter than Li in relation to the confusing information in the literature.[4] Even textbooks explaining the principles of the technique state that neither hydrogen nor helium are detectable by XPS.[5]

In XPS, photons with energies higher than 100 eV excite electrons from orbitals with a very specific binding energy, and the kinetic energy of the ejected electrons is detected with an electron energy analyzer. The binding energy is element specific, and it often contains valuable information regarding the chemical environment of the atom. In fact, the technique was originally named electron spectroscopy for chemical analysis (ESCA).[6] The highest photoionization cross section is obtained for photon energies slightly above the required energy for a particular transition.[7] With increasing energy, the cross section diminishes greatly. To measure hydrogen, the electrons in the H 1s orbitals must be excited. In atomic hydrogen, these electrons have a binding energy of 13.6 eV [8] and to maintain a reasonable cross section photon sources in the ultraviolet (UV) range are employed. For example, the cross section has a value of 1.9 Mbarn for a He1α source [7], which emits photons at 21.2 eV. With UV sources the spectra of H_2, D_2, and He have been recorded.[9, 10]

In XPS, the higher photon energy is disastrous for the H 1s photoionization cross section. To illustrate, the cross section is 5.5 and 2.8 barn for Mg Kα and Al Kα radiation sources [7, 11], respectively. This is almost 6 orders of magnitude lower than for a He 1α source. Additionally, the photon flux of typical X-ray sources is 4–5 orders of magnitude lower than that originating from a UV source, the latter being typically $10^{12\text{-}14}$ photons/s [12, 13]. Both these

facts result in an exceedingly small number of H 1s or He 1s photoelectrons, making it understandable that it was claimed, both in text books [5] and research papers [3], that it is impossible to detect hydrogen and helium using XPS. However, this is merely a technical limitation and not a fundamental one as sometimes portrayed, which often generates confusion when students try to sort through the literature on the reason behind the limitation.[4]

This letter presents experimental XPS of H 1s as well as He 1s, definitely proving that both elements can be detected in XPS. This is of tremendous academic value, as it is at odds with previous misconception.[4] The use of synchrotron radiation is crucial to observing H and He in XPS.[14] These sources commonly have photon fluxes in the order of ~10^{13} photon/s, about 3 orders of magnitude more intense compared to lab sources. Equally important, synchrotrons provide tunable photon energies, e.g., the Coherent Soft X-ray Scattering and Spectroscopy beamline (CSX-2) beamline at the National Synchrotron Light Source II (NSLS-2) has an energy range of 250–2000 eV[15, 16], putting it within the so-called "soft X-ray" energy range. At the lowest obtainable energy, the H 1s cross section is ~1 kBarn [7]. Together, the H 1s photoelectron intensity will be approximately 6 orders of magnitude higher with synchrotron-based XPS than with lab-based XPS. The ability to detect hydrogen is particularly relevant for ambient pressure (AP)-XPS. Using this approach, which was pioneered by Kai Siegbahn [17] and significantly improved in the last two decades [18-20], solid or liquid samples are being exposed to gas environments with pressures up to a few Torr [17, 21]. In this work, we took advantage of both the use of synchrotron light and AP-XPS to obtain photoelectron spectra of H_2 and He in the gas phase and H on a Pt(111) surface.

Results and Discussion

XPS of H 1s and He 1s were taken at a pressure of 0.5 Torr and they are shown in Figure 1. These gas-phase spectra were taken at the AP-XPS end station at the CSX-2 beamline of the NSLS-II.[15, 16] For diatomic molecules (e.g., H_2), photoionization normally consists of a non-dissociative and a dissociative ionization processes.[22]

$$H_2 + h\nu \rightarrow H_2^+ + e^- \quad \text{(non-dissociative)}$$
$$\rightarrow H^+ + H + e^- \quad \text{(dissociative)}$$

However, the H^+/H_2^+ ratio is relatively small, especially at the high photon energy regions. [22] The neutral hydrogen molecule has a filled bonding $1\sigma_g$ and an unoccupied antibonding $1\sigma_u^*$ molecular orbitals. In the case of non-dissociative photoionization, the XPS peak corresponds to the emission of a $1\sigma_g$ electron. Several different photoionization energies can be defined related to the various possible vibrational states of the H_2^+ cation.

$$H_2 + h\nu \rightarrow H_2^{+,\,vib} + e^-$$

As shown in Figure 1a, the broad H 1s peak is asymmetric with fine structures assigned to different vibrational transitions (see inset).[10] Note that while at first sight the fine structure appears relatively small and close to the order of magnitude of the background noise, this measurement was repeated several times and the location and separation between the features in the fine structure is reproducible. According to theoretical calculations [23], there are in total 19 different vibrational states of the hydrogen molecular ion and these are fitted in the inset in figure 1a. The full width at half maximum (FWHM) of each of these components is 0.33 eV. The first ionization energy (or the adiabatic ionization energy, v' = 0) is located at 15.41 eV, which is defined as the negative of the orbital energy of the highest occupied molecular orbital (HOMO), i.e., the minimum energy required to remove an electron from the molecule in its ground state, while the vertical ionization energy corresponds to the ionization energy associated with the transitions from the neutral ground state to different vibrational levels (ν' = 1, 2, 3...). It should be noted that the energy position in this AP-XPS spectra was calibrated according to the literature.[23] The actual measured energy is artificially higher (by 0.71-0.73 eV) than previous experimental and theoretical results [9, 10, 23] and this is due to the fact that the gas phase molecules are subjected to an electrostatic potential at the location where the ionization takes place, which is very difficult to determine and depends on various factors including the pressure of the gas and the population of ionized molecules. This has been discussed before in the AP-XPS literature.[24] In contrast, the XPS spectra of He (i.e. a monatomic species) in Figure 1b shows a sharp and symmetric peak, which has been referenced to the literature ionization energy of 24.59 eV. Note that the actual measured binding energy is 0.91 eV higher, for the same reason described above for hydrogen. The FWHM of the He 1s peak is 0.21 eV, as shown in the inset in Figure 1b. We want emphasize that a lab-based AP-XPS system would not allow these measurements given its much lower flux and lack of tunability of the photon energy, as described in more detail in the introduction section. Mass spectra were taken in order to verify the purity of the gases and to be absolutely certain that the spectra we observed corresponded indeed to hydrogen and helium.

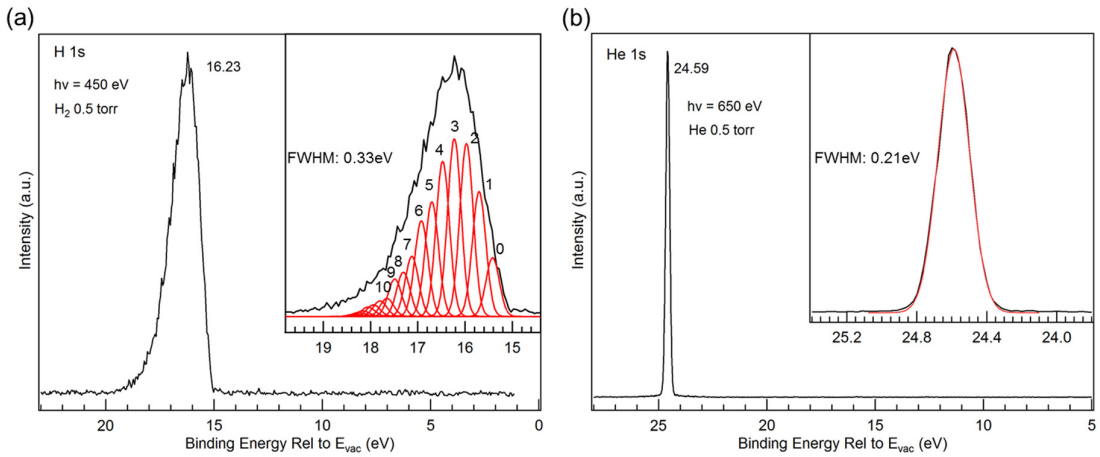

Figure 1. AP-XPS spectra of (a) H $1\sigma_g$ and (b) He 1s. The spectra were taken under 0.5 torr of H_2 (hν = 450 eV) and He (hν = 650 eV). The insets in (a) and (b) show the detailed features of the H $1\sigma_g$ and He 1s peaks. The binding energies are relative to the vacuum level (i.e., the ionization energy).

To further examine the potential of the study of hydrogen, AP-XPS measurements were performed on a Pt(111) surface. Pt(111) is an important model system for hydrogen dissociative adsorption studies.[25, 26] It is widely accepted that the dissociative adsorption of hydrogen on the Pt surface is a structure sensitive process and the binding energy strongly decreases with increasing hydrogen coverage.[27] There are only a few experimental techniques which are able to directly detect hydrogen on Pt(111), such as low-energy electron diffraction (LEED) and electron energy loss spectroscopy (EELS) [28]. Here, we examine the detailed XPS of hydrogen adsorption on Pt(111) as shown in Figure 2. Figure 2a shows in black the XPS spectrum in the valence band region obtained in ultra-high vacuum (UHV) conditions on a clean Pt(111) surface, featuring a rich d-band electronic structure near the Fermi level.[29] The Pt(111) surface was subsequently exposed to 0.5 Torr of H_2. A new feature located at a binding energy of 11.90 eV can be distinguished as shown in the red spectrum, which is assigned tentatively to hydrogen from the H-Pt bonds. This peak remains upon evacuating the hydrogen gas (green spectrum). It should be noted that no gas phase hydrogen signal can be clearly distinguished in this AP-XPS measurement, which is due to the low counts from the gas phase hydrogen when compared to the background signal. For comparison, the H 1s peak in Figure 1a is 4×10^2 cps, while the background intensity around this energy region in Figure 2a is 5×10^4 cps (both cases were obtained with the exact same analyzer settings).

Figure 2b shows the evolution of the Pt 4f spectra. Interestingly, there is a significant satellite peak located at a binding energy of 83.67 eV under 0.5 Torr H_2, which is 12.70 eV higher in

the binding energy scale than the Pt 4f peak. These peaks are probably caused by the inelastic collisions between the Pt 4f photoelectrons and the gas phase H_2 molecules (i.e., the kinetic energy of the emitted Pt 4f photoelectron from Pt(111) is reduced by the excitation of a $1\sigma_g$ electron from H_2, which has a binding energy of ~12.70 eV when referenced to the Fermi level of Pt).[24] A careful inspection of the Pt $4f_{7/2}$ further reveals indications of the adsorption of hydrogen on the Pt(111) surface as shown in the inset of Figure 2b. For clean Pt(111) surface, the lower binding energy component at 70.57 eV originates from the surface atoms, while the bulk component is located 0.4 eV above.[30] Under 0.5 Torr H_2, the surface component is significantly reduced and a new small shoulder appears at higher binding energies (71.29 eV, as shown in the deconvoluted Pt $4f_{7/2}$ region in the right panel of Figure 2b), which we tentatively assign to Pt bound to H. It should be noted that the intensity of this shoulder peak increases slightly after evacuating the H_2 gas, mostly attributed to the lower screening by H_2 gas molecules on the H-Pt surface dipoles.[31]

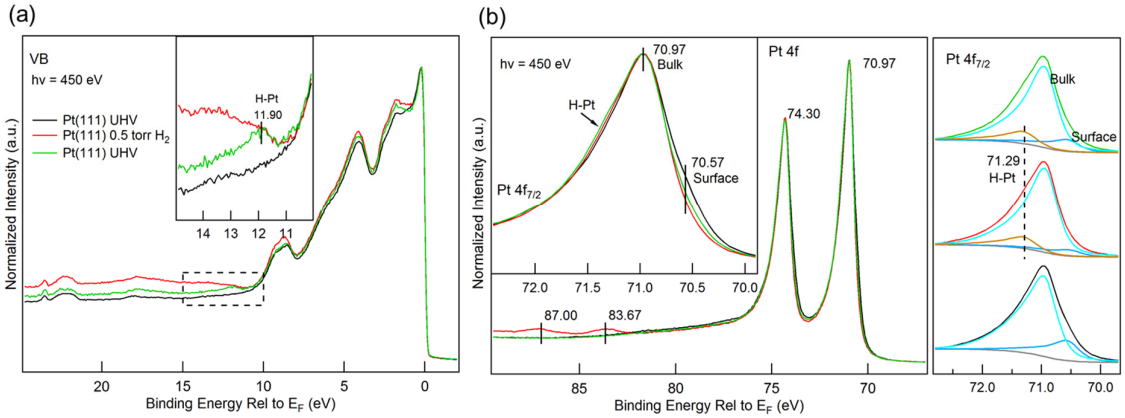

Figure 2. Hydrogen adsorption on Pt(111). XPS (a) valence band spectra and (b) Pt 4f spectra of clean Pt(111), under 0.5 Torr H_2, and after H_2 exposure at 300 K. The inset in (a) shows the detailed spectra within the dotted rectangle and the inset in (b) shows the detailed spectra of the Pt $4f_{7/2}$. (hν = 450 eV) All binding energies are relative to the Fermi level.

The peak assignments were further supported by density functional theory (DFT) calculations. DFT calculations were performed using the Vienna *Ab initio* simulation package (VASP)[32, 33]. The exchange and correlation energies were described by the PBE functional[34]. A kinetic energy cutoff of 520 eV was used, together with an 5×5×1 k-point grid for the Brillouin zone sampling. The Pt(111) substrate was modeled by five layers of Pt atoms. The top two layers of Pt atoms and H atoms were allowed to relax until forces were smaller than 0.01 eV/Å, while the bottom three layers were kept fixed. The core-level binding energies (E_{BE}) were calculated using the transition state model.[35] E_{BE} values of bulk Pt atoms were averaged over all Pt atoms in the middle three layers. As shown in Figure 3, three systems with hydrogen

coverage (Θ) of 0.25 ML, 0.50 ML and 0.75 ML were studied, corresponding to 1, 2 and 3 H atoms per unit cell (a 2 × 2 unit cell was defined). H atoms are adsorbed at the fcc hollow sites with the most negative adsorption energy (E_{ads})[36] defined as $E_{ads} = E_{Pt-H} - E_{Pt} - \frac{1}{2}E_{H_2}$, with E_{Pt-H} being the energy of the Pt (111) surface with a H atom adsorbed per unit cell, E_{Pt} the energy of the clean Pt (111) surface, and E_{H_2} the energy of a free H gas molecule. At Θ = 0.25, E_{ads} is -0.48 eV, which is consistent with published results[36]. E_{ads} of the second H atom is -0.41 eV, which is calculated by $E_{Pt-2H} - E_{Pt-H} - \frac{1}{2}E_{H_2}$, where E_{Pt-2H} is the energy of the system with a hydrogen coverage Θ = 0.50. E_{ads} of the third H atom is -0.36 eV for Θ = 0.75. The adsorption energy remains negative as the H coverage increases, indicating that the coverages of 0.25 ML, 0.50 ML and 0.75 ML give stable structures during H adsorption. Experimentally, hydrogen coverages up to 0.75 ML were achieved by dosing 0.1 - 500 L of H_2 (1L = 1.33 × 10^{-6} mbar × s) at 85 K[37].

At Θ = 0.25, the E_{BE} for clean surface Pt atoms (Pt_{surf}, red dashed circle in Fig. 3a) is 0.34 eV lower than Pt atoms in the bulk (Pt_{bulk}), which is consistent with the 0.40 eV red shift from the XPS spectra. At Θ = 0.25, the E_{BE} of Pt atoms connected with H atoms (Pt_{1H}) is 0.13 eV lower than Pt_{bulk}. At Θ = 0.50, 50% of the surface Pt atoms are bonded to 2 H atoms (Pt_{2H}). The E_{BE} of Pt_{2H} is to 0.02 eV higher than Pt_{bulk}. As Θ increases to 0.75, 25% of the surface Pt atoms are connected to 3 H atoms (Pt_{3H}). The E_{BE} of Pt_{3H} is 0.18 eV higher than Pt_{bulk}. The blue shift of Pt_{3H} from Pt_{1H} is similar to that observed in a study of hydrogen adsorption on Rh(111) where the E_{BE} shifted 0.19 eV from Rh_{1H} to Rh_{3H} as measured by XPS[38]. In the XPS spectra in Figure 2b, the Pt_H atoms are 0.32 eV higher in core level binding energies than Pt atoms in the bulk, indicating a high H coverage under the experimental conditions used in this work.

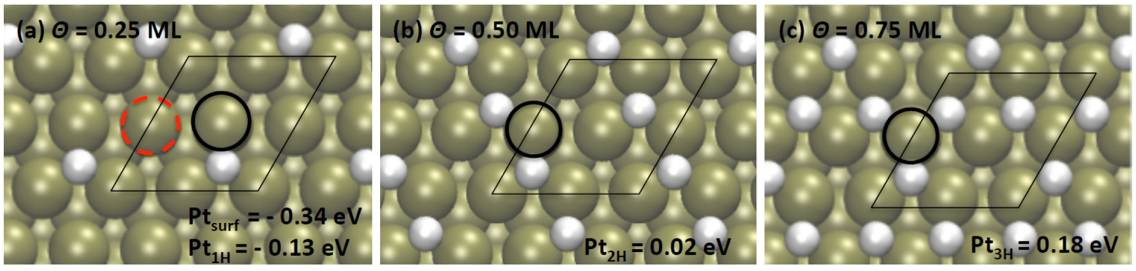

Figure 3. Top view of hydrogen adsorption structures on Pt(111) at coverage of 0.25 ML (a), 0.50 ML (b) and 0.75 ML (c). The core level binding energy shifts of surface Pt (Pt_{surf}), Pt atoms connected with 1 H atom (Pt_{1H}), Pt atoms connected with 2 H atoms (Pt_{2H}) and Pt atoms connected with 3 H atoms (Pt_{3H}) are relative to the average core level binding energies

of three Pt atom layers in the bulk. The red circle in (a) is Pt_{surf} and the black circles in (a), (b) and (c) represent Pt_{1H}, Pt_{2H} and Pt_{3H}, respectively. The rhombi represent the unit cells.

In summary, we have clearly demonstrated, by means of synchrotron-based AP-XPS measurements, that gas phase XPS spectra of hydrogen and helium can be obtained if a bright enough X-ray source is used. The H $1\sigma_g$ peak is asymmetric, which is related to the different possible vibrational modes of the final state. The He 1s peak is symmetric, as expected. In addition, we report what appears to be hydrogen adsorbed on (or dissolved in) Pt(111), as suggested by a peak at 11.9 eV during (and more clearly after) exposure to elevated pressure of hydrogen. Two other features related to hydrogen are also evident in the experiment, namely electron energy loss features in the Pt 4f and a shoulder on the higher binding energy side of the Pt $4f_{7/2}$. These results put to rest the common misconception that X-ray photoelectron spectra of elements lighter than lithium are impossible to obtain and also help in clarifying matters on the usually misunderstand the reason for this apparent impossibility. In addition, this work shows that the most abundant chemical element in the universe, namely hydrogen, can be studied with one of the most useful analytical techniques in materials science.

Acknowledgments

Research carried out in part at the Center for Functional Nanomaterials and the CSX-2 beamline of the National Synchrotron Light Source II, Brookhaven National Laboratory, supported by the U.S. Department of Energy, Office of Basic Energy Sciences, under Contract No. DE-SC0012704. J.Q. Zhong and M. Wang were supported by BNL LDRD Project No. 15-010 and W. H. Hoffmann was supported by DOE SULI program. This work was supported as part of the Integrated Mesoscale Architectures for Sustainable Catalysis (IMASC), an Energy Frontier Research Center funded by the U.S. Department of Energy, Office of Science, Basic Energy Sciences under award #DE-SC0012573. This research used resources of the National Energy Research Scientific Computing Center, a DOE Office of Science User Facility supported by the Office of Science of the U.S. Department of Energy under Contract No. DE-AC02-05CH11231.

Competing interests: The authors declare no competing financial interests.

Corresponding Authors:

*E-mail: spronsen@physics.leidenuniv.nl / mavanspronsen@fas.harvard.edu (Matthijs A. van Spronsen) and jboscoboinik@bnl.gov (J. Anibal Boscoboinik).

References

1. I. Dincer and C. Acar, International Journal of Energy Research **39** (5), 585-606 (2015).
2. F. Zhang, P. Zhao, M. Niu and J. Maddy, International Journal of Hydrogen Energy **41** (33), 14535-14552 (2016).
3. S. J. Kerber, J. J. Bruckner, K. Wozniak, S. Seal, S. Hardcastle and T. L. Barr, Journal of Vacuum Science & Technology A: Vacuum, Surfaces, and Films **14** (3), 1314-1320 (1996).
4. N. Stojilovic, Journal of Chemical Education **89** (10), 1331-1332 (2012).
5. P. van der Heide, in *X-Ray Photoelectron Spectroscopy* (John Wiley & Sons, Inc., 2011), pp. 1-12.
6. K. Siegbahn, Philosophical Transactions of the Royal Society of London. Series A, Mathematical and Physical Sciences **268** (1184), 33-57 (1970).
7. J. J. Yeh and I. Lindau, Atomic Data and Nuclear Data Tables **32** (1), 1-155 (1985).
8. J. R. Rumble, *CRC Handbook of Chemistry and Physics*, 98th ed. (CRC Press/Taylor & Francis, Boca Raton, FL., 2018).
9. M. I. Al-Joboury and D. W. Turner, Journal of the Chemical Society (Resumed) (0), 5141-5147 (1963).
10. W. J. van der Meer, H. van Lonkhuyzen, R. J. Butselaar and C. a. de Lange, The Journal of chemical physics **83**, 6173 (1985).
11. J. J. Yeh, *Atomic Calculation of Photoionization Cross-Sections and Asymmetry Parameters*. (Gordon and Breach Science Publishers, Langhorne, PE (USA), 1993).
12. https://www.prevac.eu/en/2,offer/37,instruments/120,uv-source-40a2.html, (2017).
13. http://www.scientaomicron.com/en/products/359/1231, (2017).
14. R. S. Weatherup, B. Eren, Y. Hao, H. Bluhm and M. B. Salmeron, The Journal of Physical Chemistry Letters **7** (9), 1622-1627 (2016).
15. C. Sánchez-Hanke, S. L. Hulbert, D. Shapiro and R. Reininger, Journal of Physics: Conference Series **425** (15), 152017 (2013).
16. J.-Q. Zhong, J. Kestell, I. Waluyo, S. Wilkins, C. Mazzoli, A. Barbour, K. Kaznatcheev, M. Shete, M. Tsapatsis and J. A. Boscoboinik, The Journal of Physical Chemistry C (2016).
17. H. Siegbahn and K. Siegbahn, Journal of Electron Spectroscopy and Related Phenomena **2** (3), 319-325 (1973).
18. D. F. Ogletree, H. Bluhm, G. Lebedev, C. S. Fadley, Z. Hussain and M. Salmeron, Review of Scientific Instruments **73** (11), 3872-3877 (2002).
19. D. E. Starr, Z. Liu, M. Havecker, A. Knop-Gericke and H. Bluhm, Chem. Soc. Rev. **42** (13), 5833-5857 (2013).
20. A. Shavorskiy, O. Karslioglu, I. Zegkinoglou and H. Bluhm, Synchrotron Radiation News **27** (2), 14-23 (2014).
21. M. Salmeron and R. Schlögl, Surface Science Reports **63** (4), 169-199 (2008).
22. Y. M. Chung, E. M. Lee, T. Masuoka and J. A. R. Samson, The Journal of Chemical Physics **99** (2), 885-889 (1993).

23. S. Cohen, J. R. Hiskes and R. J. Riddell, Physical Review **119** (3), 1025-1027 (1960).
24. S. Axnanda, M. Scheele, E. Crumlin, B. Mao, R. Chang, S. Rani, M. Faiz, S. Wang, A. P. Alivisatos and Z. Liu, Nano Lett. **13** (12), 6176-6182 (2013).
25. B. Poelsema, K. Lenz and G. Comsa, The Journal of Chemical Physics **134** (7), 074703 (2011).
26. M. Montano, K. Bratlie, M. Salmeron and G. A. Somorjai, Journal of the American Chemical Society **128** (40), 13229-13234 (2006).
27. P. Bene, L. Klaus and C. George, Journal of Physics: Condensed Matter **22** (30), 304006 (2010).
28. K. Christmann, G. Ertl and T. Pignet, Surface Science **54** (2), 365-392 (1976).
29. J. K. Norskov, T. Bligaard, J. Rossmeisl and C. H. Christensen, Nat Chem **1** (1), 37-46 (2009).
30. J.-Q. Zhong, X. Zhou, K. Yuan, C. A. Wright, A. Tadich, D. Qi, H. X. Li, K. Wu, G. Q. Xu and W. Chen, Nanoscale **9** (2), 666-672 (2017).
31. F. Paloukis, K. M. Papazisi, S. P. Balomenou, D. Tsiplakides, F. Bournel, J. J. Gallet and S. Zafeiratos, Applied Surface Science **423** (Supplement C), 1176-1181 (2017).
32. G. Kresse and J. Furthmüller, Physical Review B **54** (16), 11169 (1996).
33. G. Kresse and J. Furthmüller, Computational Materials Science **6** (1), 15-50 (1996).
34. J. P. Perdew, K. Burke and M. Ernzerhof, Physical review letters **77** (18), 3865 (1996).
35. C. Göransson, W. Olovsson and I. A. Abrikosov, Physical Review B **72** (13), 134203 (2005).
36. G. W. Watson, R. P. Wells, D. J. Willock and G. J. Hutchings, The Journal of Physical Chemistry B **105** (21), 4889-4894 (2001).
37. Ş. Bădescu, P. Salo, T. Ala-Nissila, S.-C. Ying, K. Jacobi, Y. Wang, K. Bedürftig and G. Ertl, Physical review letters **88** (13), 136101 (2002).
38. C. Weststrate, A. Baraldi, L. Rumiz, S. Lizzit, G. Comelli and R. Rosei, Surface science **566**, 486-491 (2004).

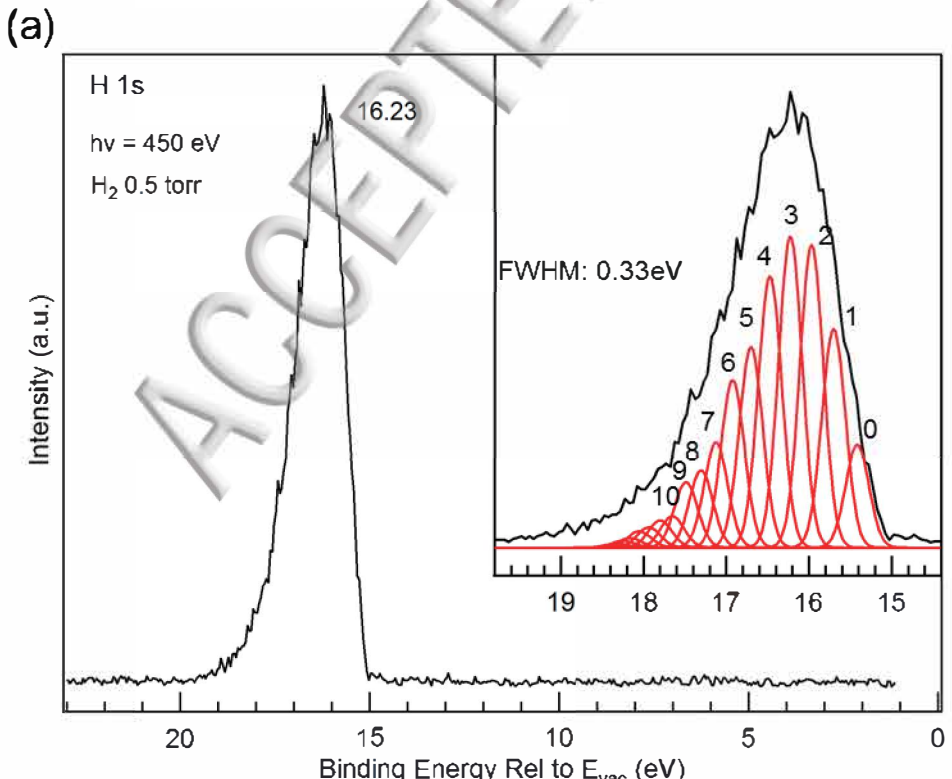
(a)
H 1s
16.23
hv = 450 eV
H2 0.5 torr
FWHM: 0.33eV
0
1
2
3
4
5
6
7
8
9
10
Intensity (a.u.)
20
15
10
5
0
19
18
17
16
15
Binding Energy Rel to Evac (eV)

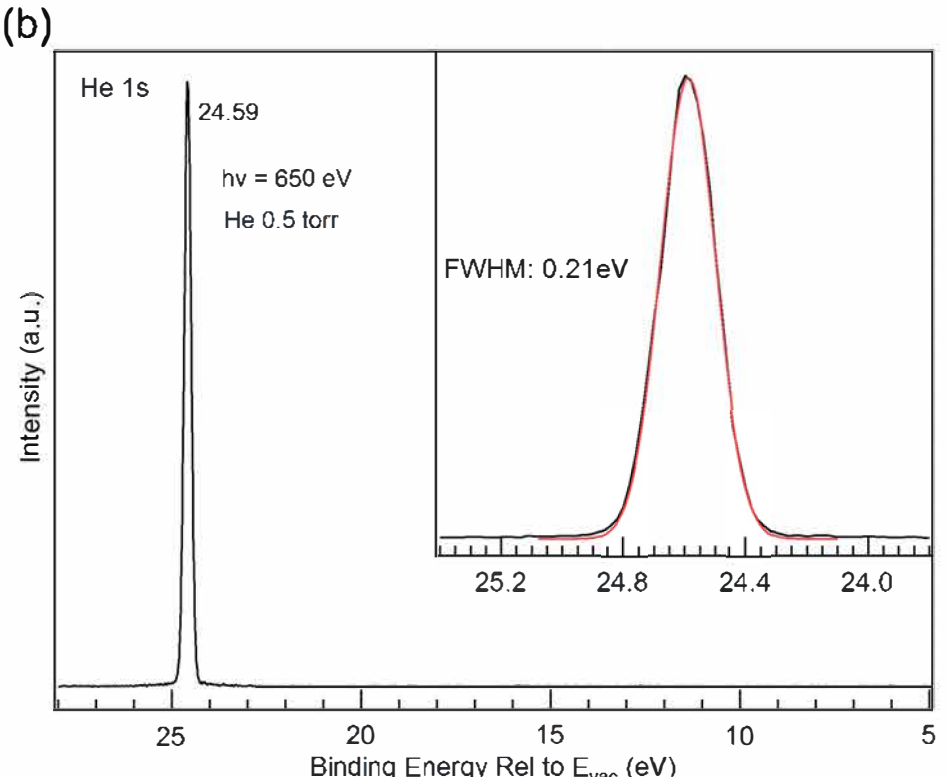
(b)
He 1s
24.59
hv = 650 eV
He 0.5 torr
FWHM: 0.21eV
Intensity (a.u.)
25
20
15
10
5
25.2
24.8
24.4
24.0
Binding Energy Rel to Evac (eV)

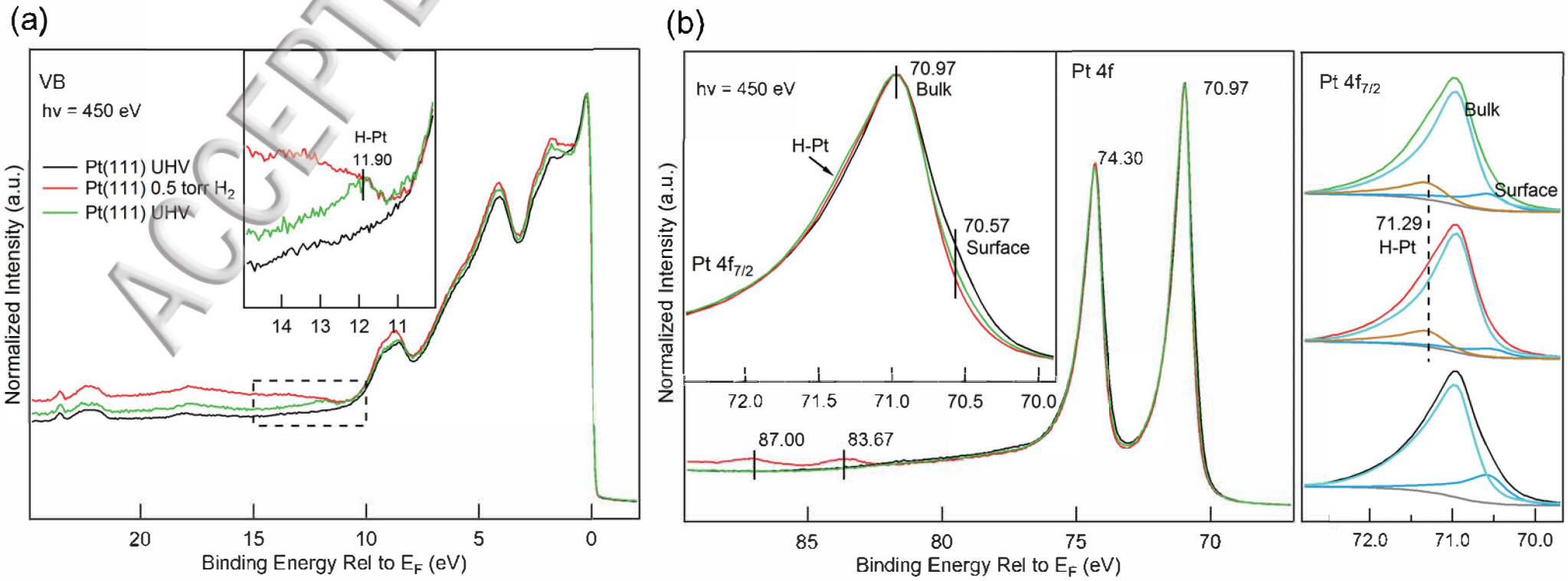
(a)
VB
hv = 450 eV
Pt(111) UHV
Pt(111) 0.5 torr H2
Pt(111) UHV
H-Pt
11.90
14 13 12 11
Normalized Intensity (a.u.)
20 15 10 5 0
Binding Energy Rel to EF (eV)
(b)
hv = 450 eV
70.97
Bulk
H-Pt
70.57
Surface
Pt 4f7/2
72.0 71.5 71.0 70.5 70.0
Pt 4f
70.97
74.30
87.00
83.67
Normalized Intensity (a.u.)
85 80 75 70
Binding Energy Rel to EF (eV)
Pt 4f7/2
Bulk
Surface
71.29
H-Pt
72.0 71.0 70.0

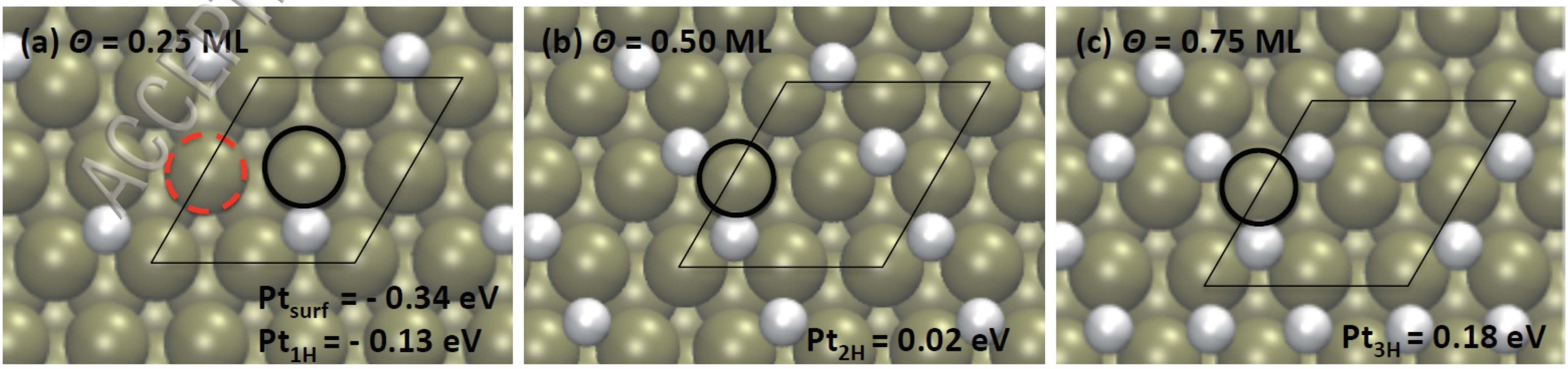
(a) Θ = 0.25 ML
Pt$_{surf}$ = - 0.34 eV
Pt$_{1H}$ = - 0.13 eV
(b) Θ = 0.50 ML
Pt$_{2H}$ = 0.02 eV
(c) Θ = 0.75 ML
Pt$_{3H}$ = 0.18 eV